

Mixed Convection of a Nanofluid in a Vertical Anisotropic Porous Channel with Heated/Cooled Walls

S. Slama¹, H. Kahalerras¹ and B. Fersadou¹

Abstract: A numerical study is conducted to investigate the problem of mixed convection of a nanofluid in a vertical porous channel with one wall heated and the other cooled. The Darcy-Brinkman-Forchheimer model is used to describe the flow in the porous medium, considered as anisotropic in thermal conductivity, and the two-phase approach is adopted to simulate the motion of the nanofluid. The governing equations with the associated boundary conditions are solved by the finite volume method. The parametric study is focused on the variation of the Richardson number Ri , the heat fluxes ratio R_q , the Darcy number and the thermal conductivity ratio λ characterizing the anisotropy. The results revealed that the heat transfer rates for both channel walls increase with λ and decrease with Da . The mean Nusselt number for the heated wall increases with the rise of Ri and R_q , while that for the cooled wall evolves in opposite direction. In addition, it is found that the dynamical and thermal fields become extremely sensitive to the variations of the various parameters mentioned above when reverse flow appears. For this reason, maps showing the situations of occurrence of this phenomenon are performed.

Keywords: Mixed convection, nanofluid, anisotropic porous medium, reverse flow.

Nomenclature

C	Inertial coefficient
C_p	Specific heat at constant pressure ($J \cdot kg^{-1} \cdot K^{-1}$)
Da	Darcy number
D_B	Brownian diffusion coefficient ($m^2 \cdot s^{-1}$)
D_T	Thermophoretic diffusion coefficient ($m^2 \cdot s^{-1}$)
g	Gravitational acceleration ($m \cdot s^{-2}$)
H	Channel width (m)
k	Thermal conductivity ($W \cdot m^{-1} \cdot K^{-1}$)
K	Intrinsic permeability of the porous medium (m^2)
ℓ	Channel length (m)
Le	Lewis number
N_B	Brownian motion parameter
N_R	Buoyancy ratio parameter

¹ Faculty of Mechanical and Process Engineering, Houari Boumediene University of Sciences and Technology (USTHB), B. P. 32, El Alia, Bab Ezzouar 16111, Algiers-Algeria

N_T	Thermophoresis parameter
Nu	Nusselt number
p	Pressure (Pa)
Pr	Prandtl number
q	Heat flux ($\text{W}\cdot\text{m}^{-2}$)
Re	Reynolds number
Ri	Richardson number
R_k	Thermal conductivity ratio
R_q	Heat flux ratio
R	Viscosity ratio
T	Temperature (K)
u	Axial velocity ($\text{m}\cdot\text{s}^{-1}$)
v	Transverse velocity ($\text{m}\cdot\text{s}^{-1}$)
x	Axial coordinate (m)
y	Transverse coordinate (m)

Greek symbols

	Thermal expansion coefficient (K^{-1})
	Porosity
	Dimensionless temperature
	Anisotropic thermal conductivity ratio
	Viscosity ($\text{kg}\cdot\text{m}^{-1}\cdot\text{s}^{-1}$)
	Density ($\text{kg}\cdot\text{m}^{-3}$)
	Dimensionless nanoparticle volume fraction
	Nanoparticle volume fraction

Subscripts

c	Cooled
$effx$	Effective in the axial direction
$effy$	Effective in the transverse direction
f	Fluid
h	Heated
i	Inlet
m	Mean
p	Nanoparticle
w	Wall

1 Introduction

Mixed convection flow in a channel filled with a porous medium has been widely studied over the last decades [Hadim and Chen (1994); Chen, Chung, Wu et al. (2000); Degan and Vasseur (2002); Umavathi, Kumar, Chamkha et al. (2005); Bera and Khalili (2007); Barletta, Magyari, Pop et al. (2008); Cimpean, Pop, Ingham et al. (2009)] due to the presence of such material in various engineering applications including solid-matrix heat

exchangers, building thermal insulation, geothermal systems, solar collectors, drying processes, and so on. A comprehensive review of the literature relating to this subject can be found in the recent book of Nield et al. [Nield and Bejan (2013)]. Recently, Jha et al. [Jha, Daramola and Ajibade (2015, 2016)] obtained analytical solution for steady-periodic regime of a fully developed mixed convection flow in inclined parallel-plates channel and vertical tube filled with porous material and subjected to time-periodic boundary conditions. Nanofluid, a term firstly introduced by Choi [Choi (1995)], is a suspension of solid nanoparticles (1-100 nm) at very low volume fraction in a base fluid. This new class of fluids, forms a very stable colloidal system which will prevent rapid settling and will reduce clogging in the walls of heat transfer devices. Due to their thermal properties superior to those of conventional fluids, the nanofluids can be used to enhance the performance of thermal systems in several engineering applications such as heat exchangers, cooling devices, chemical processes, and so on. Single phase and two-phase approach have been used in the literature to study convective heat transfer with nanofluids. In the first approach, the nanofluid is considered as single-phase fluid which means that both the base fluid and nanoparticles are in thermal equilibrium and no slip motion occurs between the solid and liquid phases. The two-phase model, proposed by Buongiorno [Buongiorno (2006)], is based on the concept of a relative velocity between the nanoparticles and the base fluid. After considering seven slip mechanisms: inertia, Brownian diffusion, thermophoresis, diffusiophoresis, Magnus effect, fluid drainage and gravity settling, he concluded that in the absence of turbulent effects it is the Brownian diffusion and thermophoresis that will be important. On the basis of the mathematical model proposed by Buongiorno [Buongiorno (2006)], Nield et al. [Nield and Kuznetsov (2009a, 2009b, 2011a, 2011b, 2011c)], Kuznetsov et al. [Kuznetsov and Nield (2010, 2014)] conducted a series of studies on viscous fluids and porous media. Since then, a considerable number of research works on nanofluid convection have been performed, e.g. [Xu, Fan and Pop (2013); Yang, Li and Nakayama (2013); Malvandi and Ganji (2014, 2015)]. The effects of Brownian motion and thermophoresis on fluid flow and heat transfer characteristics by adding a porous material have also been considered. Hajipour et al. [Hajipour and Dehkordi (2012)] analyzed both analytically and numerically the problem of fully-developed mixed convective heat transfer of nanofluids in a vertical channel partly filled with porous medium for constant temperature boundary condition and by taking into account viscous dissipation. The authors found that the use of nanofluids improves significantly the heat transfer process. The effect of nanoparticles migration on forced convective flow of nanofluids flowing through a porous channel was investigated numerically by Maghrebi et al. [Maghrebi, Nazari and Armaghani (2012)]. The results showed a decrease in the local Nusselt number with the increase of the Lewis number and the Brownian motion parameter. A numerical analysis of steady natural convection heat transfer in a square porous cavity filled by a nanofluid with solid walls of finite thickness was carried out by Sheremet et al. [Sheremet and Pop (2014)]. Non-homogeneous distribution of the nanoparticles was obtained at high thermophoresis parameter, low Brownian motion parameter, low Lewis and Rayleigh numbers, and high thermal conductivity ratio. Matin et al. [Matin and Ghanbari (2014)] studied the fully-developed mixed convection flow of nanofluids through a vertical porous channel with the walls at different constant temperatures. Viscous dissipation was taken into account, and the governing equations were solved both analytically and numerically.

The amplitude and extents of the reversal flow increase with the augmentation of the buoyancy force intensity, the Brinkman number, the thermophoresis parameter, and the diminution of the buoyancy ratio parameter. The onset of penetrative convection in a horizontal, anisotropic Brinkman porous layer saturated by a nanofluid was investigated by Shivakumara et al. [Shivakumara and Dhananjaya (2015)]. They found that the increase of Darcy number and thermal anisotropy parameter have the effect of delaying the onset of convection.

Despite the large number of studies on convective heat transfer in porous media filled with nanofluids, this topic remains not completely investigated and therefore requires more exploration. The main objective of this paper is the study of mixed convection of nanofluid in a vertical porous channel with one wall heated and the other cooled. The two-phase model is used to describe the nanofluid motion and the porous medium is considered to be anisotropic in thermal conductivity.

2 Mathematical formulation

The physical domain under investigation, shown in Fig. 1, is a vertical parallel-plates channel with spacing H , length ℓ , and filled with a nanofluid-saturated porous medium. The wall $y=0$ is heated at a constant heat flux q_h , while the wall $y=H$ is cooled at a rate q_c . The nanofluid enters the channel at a uniform velocity U_i , constant temperature T_i and nanoparticles volume fraction ϕ_i .

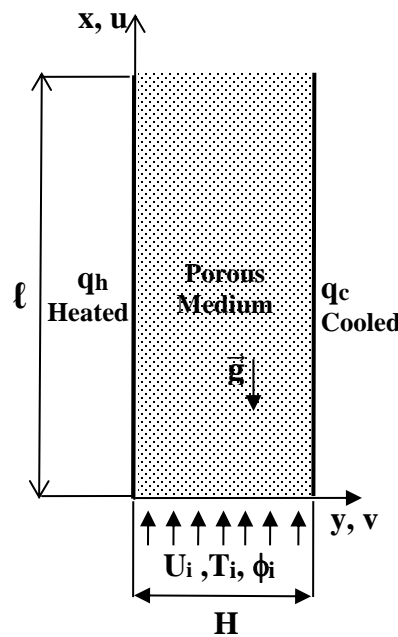


Figure 1: Physical domain

The mixed convection flow is incompressible, steady-state, laminar and two-dimensional with no internal heat generation and neglecting viscous dissipation. The nanofluid is Newtonian and

is treated as a two-component non-homogeneous mixture (base fluid plus nanoparticles). The nanoparticles, of smaller size than that of the matrix pores, are suspended in the nanofluid using either surfactant or surface change technology, preventing the agglomeration and deposition of these on the porous matrix. The porous medium is considered to be homogeneous but anisotropic in thermal conductivity. The nanoparticles, base fluid, and porous medium are locally in thermal equilibrium with their thermophysical properties taken to be constant except the density variation in the buoyancy force which is determined by using the Boussinesq approximation.

Based on the above assumptions, and using the modified Brinkman-Forchheimer extended model for the flow in the porous medium in combination with the nanofluid model proposed by Buongiorno [Buongiorno (2006)] to take into account the effects of Brownian motion and thermophoresis [Nield and Kuznetsov (2009b)], the conservation equations of mass, momentum, energy and nanoparticles volume fraction can be expressed in the following manner:

Continuity

$$\frac{\partial u}{\partial x} + \frac{\partial v}{\partial y} = 0 \quad (1)$$

Momentum

$$\begin{aligned} \frac{\rho_f}{\varepsilon^2} \vec{V} \cdot \nabla \vec{V} = -\nabla p + \mu_{eff} \nabla^2 \vec{V} - \frac{\mu_f}{K} \vec{V} - \rho_f \frac{C}{\sqrt{K}} |\vec{V}| \vec{V} \\ + \left\{ \phi \rho_p + (1 - \phi) \rho_f \left[1 - \beta_f (T - T_i) \right] \right\} \vec{g} \end{aligned} \quad (2)$$

Assuming a dilute mixture and using a suitable choice for the reference pressure, the momentum equation can be linearized as Nield et al. [Nield and Kuznetsov (2009b)] did. Eq. (2) becomes:

x-Momentum

$$\begin{aligned} \frac{\rho_f}{\varepsilon^2} \left(u \frac{\partial u}{\partial x} + v \frac{\partial u}{\partial y} \right) = -\frac{\partial p}{\partial x} + \mu_{eff} \left(\frac{\partial^2 u}{\partial x^2} + \frac{\partial^2 u}{\partial y^2} \right) - \frac{\mu_f}{K} u - \rho_f \frac{C}{\sqrt{K}} |\vec{V}| u \\ + \left\{ (1 - \phi_i) \rho_f \beta_f (T - T_i) - (\rho_p - \rho_f) (\phi - \phi_i) \right\} g \end{aligned} \quad (3a)$$

y-Momentum

$$\frac{\rho_f}{\varepsilon^2} \left(u \frac{\partial v}{\partial x} + v \frac{\partial v}{\partial y} \right) = -\frac{\partial p}{\partial y} + \mu_{eff} \left(\frac{\partial^2 v}{\partial x^2} + \frac{\partial^2 v}{\partial y^2} \right) - \frac{\mu_f}{K} v - \rho_f \frac{C}{\sqrt{K}} |\vec{V}| v \quad (3b)$$

Energy

$$\begin{aligned}
(\rho C_p)_f \left(u \frac{\partial T}{\partial x} + v \frac{\partial T}{\partial y} \right) &= \left(k_{effx} \frac{\partial^2 T}{\partial x^2} + k_{effy} \frac{\partial^2 T}{\partial y^2} \right) \\
&+ \varepsilon (\rho C_p)_p \left[D_B \left(\frac{\partial \phi}{\partial x} \frac{\partial T}{\partial x} + \frac{\partial \phi}{\partial y} \frac{\partial T}{\partial y} \right) + \frac{D_T}{T_i} \left(\left(\frac{\partial T}{\partial x} \right)^2 + \left(\frac{\partial T}{\partial y} \right)^2 \right) \right]
\end{aligned} \quad (4)$$

Nanoparticle volume fraction

$$\frac{1}{\varepsilon} \left(u \frac{\partial \phi}{\partial x} + v \frac{\partial \phi}{\partial y} \right) = D_B \left(\frac{\partial^2 \phi}{\partial x^2} + \frac{\partial^2 \phi}{\partial y^2} \right) + \frac{D_T}{T_i} \left(\frac{\partial^2 T}{\partial x^2} + \frac{\partial^2 T}{\partial y^2} \right) \quad (5)$$

The associated boundary conditions are:

$$u = U_i, v = 0, T = T_i, \phi = \phi_i \text{ at } x=0 \quad (6)$$

$$\frac{\partial u}{\partial x} = 0, v = 0, \frac{\partial T}{\partial x} = 0, \frac{\partial \phi}{\partial x} = 0 \text{ at } x=\ell \quad (7)$$

$$u = 0, v = 0, \frac{\partial T}{\partial y} = -\frac{q_h}{k_{effy}}, D_B \frac{\partial \phi}{\partial y} = -\frac{D_T}{T_i} \frac{\partial T}{\partial y} \text{ at } y=0 \quad (8)$$

$$u = 0, v = 0, \frac{\partial T}{\partial y} = -\frac{q_c}{k_{effy}}, D_B \frac{\partial \phi}{\partial y} = -\frac{D_T}{T_i} \frac{\partial T}{\partial y} \text{ at } y=H \quad (9)$$

Using the following dimensionless variables

$$X = \frac{x}{H}; Y = \frac{y}{H}; U = \frac{u}{U_i}; V = \frac{v}{U_i}; P = \frac{p}{\rho U_i^2}; \theta = \frac{T - T_i}{q_h H / k_f}; \varphi = \frac{\phi - \phi_i}{\phi_i}$$

we obtain the following conservation equations and boundary condition in dimensionless form:

$$\frac{\partial U}{\partial X} + \frac{\partial V}{\partial Y} = 0 \quad (10)$$

$$U \frac{\partial U}{\partial X} + V \frac{\partial U}{\partial Y} = -\frac{\partial P}{\partial X} + \frac{R_\mu}{\text{Re}} \left(\frac{\partial^2 U}{\partial X^2} + \frac{\partial^2 U}{\partial Y^2} \right) - \frac{1}{\text{Re Da}} U - \frac{C}{\sqrt{\text{Da}}} |\vec{V}| U + \text{Ri} (\theta - N_R \varphi) \quad (11)$$

$$U \frac{\partial \theta}{\partial X} + V \frac{\partial \theta}{\partial Y} = \frac{R_k}{\text{Re Pr}} \left(\frac{\partial^2 \theta}{\partial X^2} + \lambda \frac{\partial^2 \theta}{\partial Y^2} \right) + \frac{1}{\text{Re Pr}} \left[N_B \left(\frac{\partial \phi}{\partial X} \frac{\partial \theta}{\partial X} + \frac{\partial \phi}{\partial Y} \frac{\partial \theta}{\partial Y} \right) + N_T \left(\left(\frac{\partial \theta}{\partial X} \right)^2 + \left(\frac{\partial \theta}{\partial Y} \right)^2 \right) \right] \quad (12)$$

$$U \frac{\partial \phi}{\partial X} + V \frac{\partial \phi}{\partial Y} = \frac{1}{\text{Le Re Pr}} \left(\frac{\partial^2 \phi}{\partial X^2} + \frac{\partial^2 \phi}{\partial Y^2} \right) + \frac{N_T}{N_B} \frac{1}{\text{Le Re Pr}} \left(\frac{\partial^2 \theta}{\partial X^2} + \frac{\partial^2 \theta}{\partial Y^2} \right) \quad (13)$$

$$U = 1, V = 0, \theta = 0, \phi = 0 \text{ at } X=0 \quad (14)$$

$$\frac{\partial U}{\partial X} = 0, V = 0, \frac{\partial \theta}{\partial X} = 0, \frac{\partial \phi}{\partial X} = 0 \text{ at } X=L \quad (15)$$

$$U = 0, V = 0, \frac{\partial \theta}{\partial Y} = -\frac{1}{R_k \lambda}, \frac{\partial \phi}{\partial Y} = -\frac{N_T}{N_B} \frac{\partial \theta}{\partial Y} \text{ at } Y=0 \quad (16)$$

$$U = 0, V = 0, \frac{\partial \theta}{\partial Y} = -\frac{R_q}{R_k \lambda}, \frac{\partial \phi}{\partial Y} = -\frac{N_T}{N_B} \frac{\partial \theta}{\partial Y} \text{ at } Y=1 \quad (17)$$

The dimensionless parameters appearing in the previous equations and boundary conditions are defined as:

$$\text{Re} = \frac{U_i H \rho_f}{\mu_f}; Da = \frac{K}{H^2}; R_\mu = \frac{\mu_{eff}}{\mu_f}; Ri = \frac{(1-\phi_i) g \beta_f (q_h H / k_f) H^3}{(\mu_f / \rho_f)^2} \frac{1}{\text{Re}^2}; N_R = \frac{\phi_i (\rho_p - \rho_f)}{(1-\phi_i) \rho_f \beta (q_h H / k_f)}$$

$$\text{Pr} = \frac{\mu_f C p_f}{k_f}; R_k = \frac{k_{effx}}{k_f}; \lambda = \frac{k_{effy}}{k_{effx}}; N_B = \varepsilon D_B \frac{(\rho C p)_p}{k_f} \phi_i; N_T = \varepsilon \frac{D_T}{T_i} \frac{(\rho C p)_p}{k_f} \frac{q_h H}{k_f}; Le = \frac{k_f}{\varepsilon D_B (\rho C p)_f}$$

$$Rq = \frac{q_c}{q_h}$$

The local Nusselt numbers at the heated and cooled walls of the channel are evaluated as follows:

$$Nu_h = \frac{q_h H}{(T_{wh} - T_i) k_f} = \frac{1}{\theta_{wh}}; Nu_c = \frac{q_c H}{(T_i - T_{wc}) k_f} = -\frac{R_q}{\theta_{wc}} \quad (18)$$

The average Nusselt numbers are defined as:

$$Nu_{m(h,c)} = \frac{1}{L} \int_0^L Nu_{(h,c)} dX \quad (19)$$

3 Numerical procedure

The finite volume method (1980) is used to solve the governing Eqs. (10-13) with the associated boundary conditions (14-17) employing a pressure-velocity formulation. The power law scheme is employed in the discretizing procedure to treat the convection and diffusion terms. The Brownian and thermophoresis terms in Eq. (12) are approximated with a first order forward difference, whereas the source term in Eq. (13) is discretized using a second order central finite difference. The obtained algebraic equations are solved using the line by line technique, combining between the tridiagonal matrix algorithm and the Gauss-Seidel method. A non-uniform grid is employed in the transverse direction by locating the finer meshes with the finer meshes placed near the walls of the channel. To analyze the effect of the grid size on the numerical solution, several grid systems are tested for various combinations of the controlling parameters. A typical test is shown in Tab. 1 and a grid system of 250×50 (in X and Y directions, respectively) is adopted since the relative errors on the mean Nusselt numbers are less than 0.5%. For the convergence criteria of the iterative process, the relative variations of velocity components, temperature and concentration between two successive iterations are required to be smaller than 10^{-6} . As the simulation time and the error evolve in opposite directions; So, trial calculations were necessary to optimize the computation time and accuracy. To validate the elaborated computational code, comparison is made with the results of Desrayaud et al. [Desrayaud and Lauriat (2009)] concerning the problem of laminar mixed convection in a symmetrically heated, vertical plate channel. The velocity and temperature profiles, at various positions in the channel, illustrated in Fig. 2 shows a very good agreement.

Table 1: Grid sensitivity analysis for $Da=10^{-2}$, $Ri=10$, $R_q=1.25$ and $\lambda=0.75$

Grid number (X×Y)	100×20	150×30	200×40	250×50	300×60
Nu_{mh}	8.204	8.033	8.047	8.028	8.015
Relative error (%)	-	2.08	0.17	0.24	0.16
Nu_{mc}	1.308	1.367	1.391	1.395	1.401
Relative error (%)	-	4.51	1.75	0.29	0.43

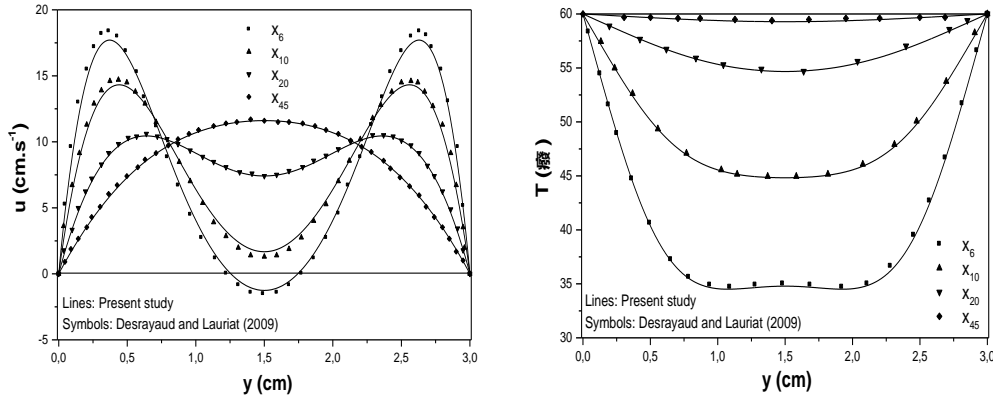


Figure 2: Axial velocity profiles and temperature distributions for various positions in the channel: $Re=300$, $Ri=1.77$

4 Results

All computations are performed by keeping fixed the channel length ($L=30$), the Reynolds number ($Re=100$), the Prandtl number ($Pr=7$ to model water as the base fluid), the Lewis number ($Le=1$), the buoyancy ratio parameter ($N_R=0.1$), the Brownian motion parameter ($N_B=0.1$), the thermophoresis parameter ($N_T=0.1$), the porosity ($\epsilon=0.9$ for metal foams), the inertial coefficient ($C=0.1$, value used in a large number of research works dealing with porous media), the viscosity ratio ($R_\mu=1$, since the value of the effective viscosity in the Brinkman's extension remains controversial, it is taken to be the same as the base fluid viscosity as a first approximation) and the thermal conductivity ratio ($R_k=1$). The parametric study is focused on the effects of the buoyancy force intensity ($0 \leq Ri \leq 20$), the heat flux ratio ($0.25 \leq R_q \leq 2$), the porous medium permeability ($10^{-6} \leq Da \leq 10^{-1}$), and the anisotropic thermal conductivity ratio ($0.5 \leq \lambda \leq 5$) on the profiles of the axial velocity, temperature and nanoparticles volume fraction, as well as the mean Nusselt numbers for both channel walls.

The stream-wise velocity, temperature and nanoparticles volume fraction profiles at the channel exit for different values of the Richardson number are depicted on Fig. 3. The symmetry of the velocity profile obtained at $Ri=0$, corresponding to the case of forced convection, disappears with the intensification of the buoyancy force which acts in the same direction of the nanofluid motion at the heated wall and in the opposite direction at the level of the cooled plate. This will cause an acceleration of the nanofluid flow near the heated zone and its slowing down in the cooled region. This asymmetry is all the more important as the buoyancy force intensity is increasing. When Ri exceeds the threshold of 12, the velocity values become negative in the region adjacent to the cooled wall so that there is appearance of reverse flow and the nanofluid moves downward in this zone.

Reverse flow in asymmetrically heated vertical channels was considered numerically and experimentally by numerous researchers. This kind of flow was observed experimentally for the first time by Sparrow et al. [Sparrow, Chrysler and Azevedo (1984)]. Augun et al. [Augun and Worku (1986)], and Cheng et al. [Cheng, Kou and Huang (1990)] developed

criteria and presented maps of its occurrence. Habib et al. [Habib, Said, Ahmed et al. (2002)] carried out velocity measurements to highlight this phenomenon. Two types of flow behaviors, with and without fluid recirculation, were considered by Ameziani et al. [Ameziani, Bouhadef, Bennacer et al. (2008)] in a vertical opened porous cylinder. The effect of surface radiation was considered by Li et al. [Li, Boussetta, Chénier et al. (2013)]. Recently and in order to improve heat transfer, Fu et al. [Fu, Chao, Wu and Lin (2016)] proposed a new method that can eliminate flow reversal. All these studies demonstrated that reverse flow is a result of high intensity of buoyancy force, intense natural convection and/or asymmetrical heating.

The temperature and nanoparticles volume fraction profiles evolve in opposite directions. The nanofluid is heated ($\theta > 0$) at the hot wall and cooled ($\theta < 0$) at the cold plate. These temperature gradients lead to migration of nanoparticles from the heated region ($\varphi < 0$) to the cooled region ($\varphi > 0$) resulting in a non-uniform distribution of φ . Increasing Ri leads to a reduction of and so an increase of near the two walls. In fact, by raising the intensity of the buoyancy force there is acceleration of the fluid motion at the level of the heated plate leading to a better cooling of the nanofluid, whereas in the vicinity of the cold plate the intensification of the reversal flow results in more cooling.

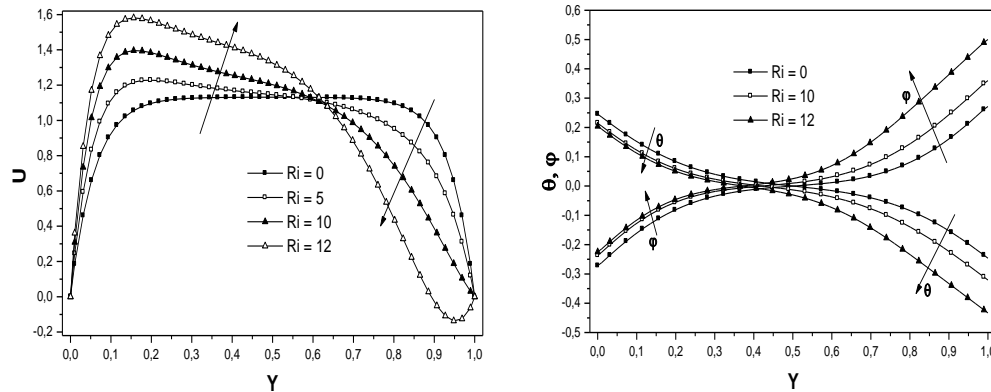
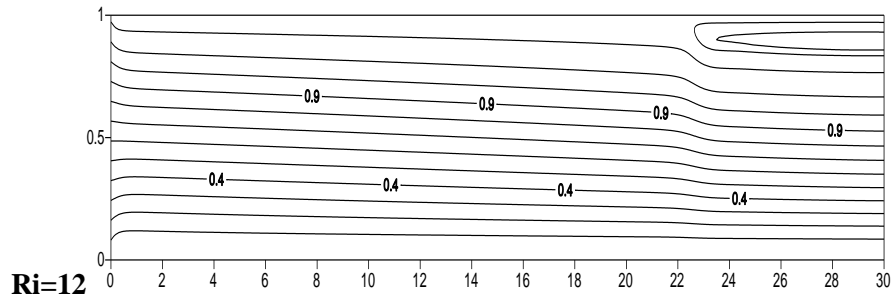


Figure 3: Profiles of U , θ and φ at channel exit for different values of Ri , $Da=10^{-2}$, $R_q=1$ and $\lambda=1$

To better highlight the reverse flow phenomenon, we have present in Fig. 4 the streamlines for two different Richardson numbers. As Ri increases, the effect of buoyancy force and free convection gets stronger causing appearance of re-circulative flow near the cooled wall whose magnitude and extent rises with this parameter.



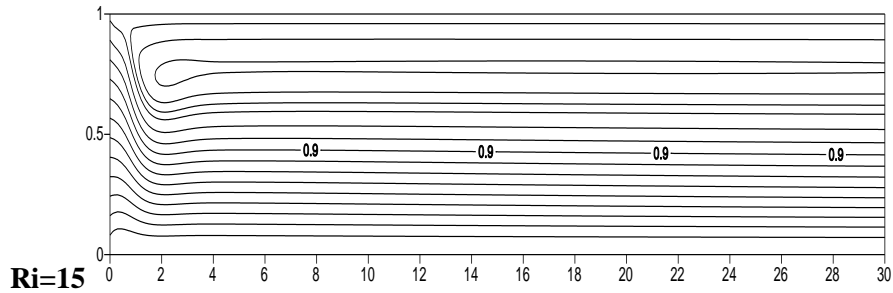


Figure 4: Streamlines for different values of Ri, $Da=10^{-2}$, $R_q=1$ and $\lambda=1$

Fig. 5 depicted the variation of mean Nusselt numbers Nu_{mh} and Nu_{mc} with Richardson number. For the heated plate, the heat transfer occurs from the channel wall to the nanofluid whereas for the cooled plate, the heat transfer direction is from the nanofluid to the wall. It appears that the heat transfer rate is enhanced at the hot wall with the increase of the Richardson number and is diminished at the cool wall. This is justified by the acceleration of the nanofluid motion near the hot plate and its slowing down on the cold plate side as a result of the increase in the intensity of the buoyancy force. It should also be noted that these variations with Ri become very apparent beyond $Ri=12$; threshold value from which the reverse flow occurs near the cooled channel wall.

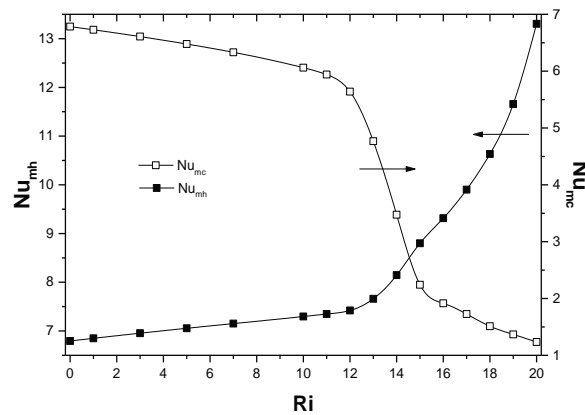


Figure 5: Variation of Nu_m with Ri for $Da=10^{-2}$, $R_q=1$ and $\lambda=1$

Fig. 6 and Fig. 7 show how the heat flux ratio R_q can affect the different characteristics of flow and heat transfer. The Richardson number being linked to the heating flux q_h and being kept fixed; any variation of R_q will be related to that of the cooling flux q_c . The heat flux ratio seems to have similar behavior to that of Ri, where its increasing has the consequence of slowing down the nanofluid motion in the vicinity of the cooled wall and its acceleration near the heated plate in order to maintain a constant flow rate. The reverse flow begins to settle at the level of the right wall for a value of the heat flux ratio around 1.2. The increase of the cooling flux q_c leads to a decrease of the nanofluid temperature and this effect is more apparent beside the cooled plate with its propagation more and more towards the center of the channel. Further to these strong temperature gradients and under the thermophoresis effect, the nanoparticles migrate towards the cooled region and their

accumulation is all the greater as the value of R_q increases. As consequences to what have been said before, Nu_{mh} and Nu_{mc} increases and decreases respectively with the heat flux ratio slightly at the beginning, before that these two evolutions become considerable from the threshold value for which there is appearance of the reverse flow.

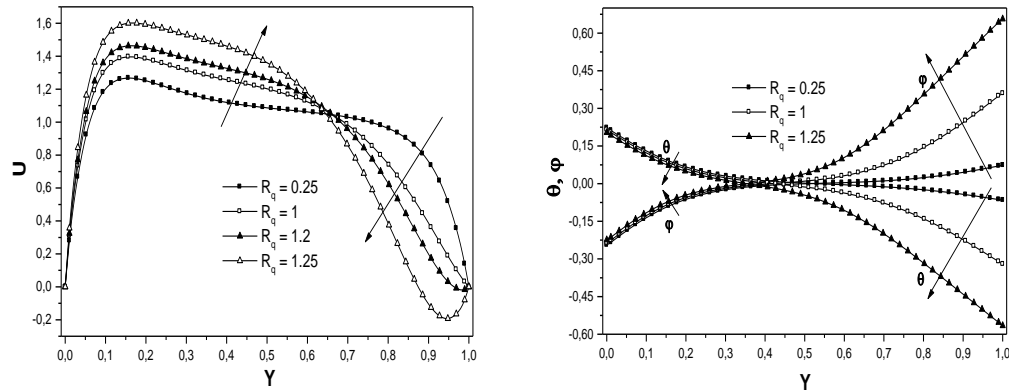


Figure 6: Profiles of U , θ and ϕ at channel exit for different values of R_q , $Da=10^{-2}$, $Ri=10$ and $\lambda=1$

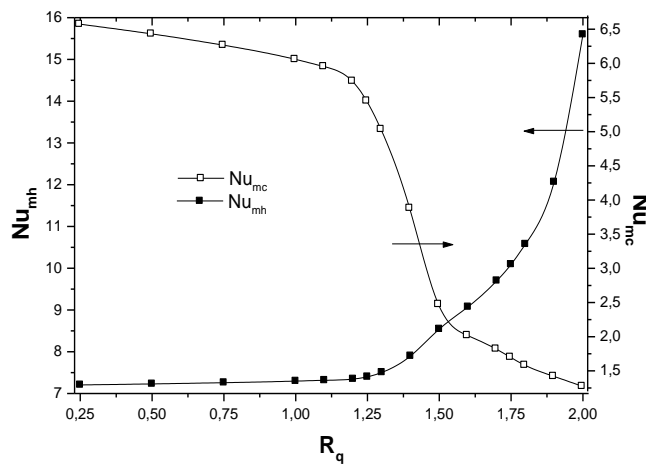


Figure 7: Variation of Nu_m with R_q for $Da=10^{-2}$, $Ri=10$ and $\lambda=1$

The effects of porous medium permeability on the velocity, temperature and nanoparticles volume fraction profiles are displayed on Fig. 8. At low Darcy number, the porous medium creates a high resistance to flow and the distribution of the velocity is uniform transversely with a flattened profile at the center. When Da increases, the resistance is lower and the nanofluid flows more easily into the porous medium with its acceleration near the heated wall and its slowing down in the vicinity of the cooled cold plate under the effect of gravity. The reverse flow near the cold wall of the channel appears only from Da around 0.06. The increase in the mobility of the nanofluid with the augmentation of the porous medium permeability resulted in the reduction of θ and the increase of ϕ ; such behavior is more perceptible in the vicinity of the cooled plate.

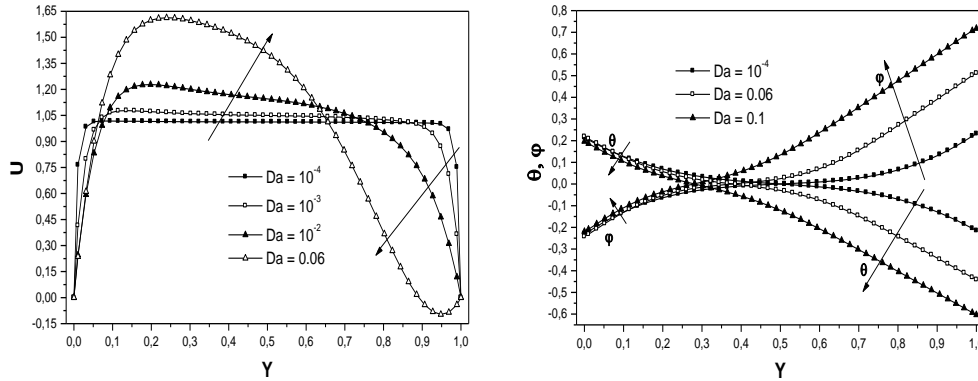


Figure 8: Profiles of U , θ and ϕ at channel exit for different values of Da , $Ri=5$, $R_q=1$ and $\lambda=1$

As expected and as found in several previous studies in porous medium, both the Nusselt numbers decrease with the increase of the Darcy number due to the reduction of the velocity gradients in the vicinity of the canal walls (Fig. 9). However, from $Da \approx 0.06$ there is a change in the evolution of Nu_{mh} where the heat transfer rate begins to improve due to the appearance of the reverse flow which has led to an acceleration of the nanofluid motion near the hot plate.

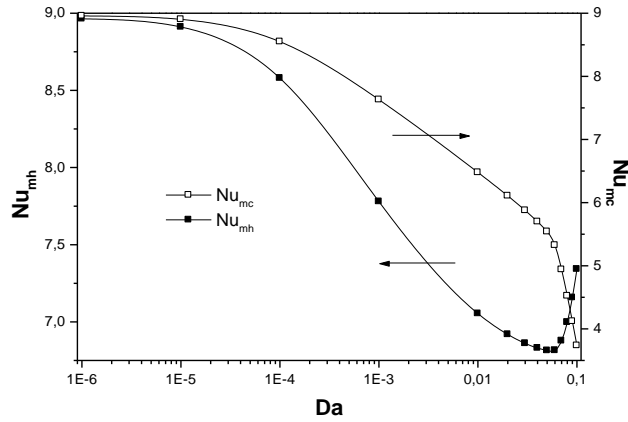


Figure 9: Variation of Nu_m with Da for $Ri=5$, $R_q=1$ and $\lambda=1$

So, far the porous medium has been considered as isotropic and it will be interesting to study the influence of thermal anisotropy (Fig. 10 and Fig. 11). Increasing the anisotropic thermal conductivity ratio is equivalent to raise the value of the transverse effective thermal conductivity k_{effy} . When $\lambda < 1$, the heat generated at the left plate is badly evacuated in the transverse direction. Due to its accumulation and under the effect of the buoyancy force, the nanofluid is accelerated in this zone, and in order to conserve the flow rate, it is decelerated in the vicinity of the right plate. The reverse flow in the channel appears for values of the anisotropic thermal conductivity ratio less or equal to approximately 0.75. When the transverse thermal conductivity k_{effy} increases, the heat evacuation is improved and the nanofluid temperature at the heated plate decreases giving rise to a buoyancy force

of lower intensity and thus a lesser increase in velocity and disappearance of the reverse flow. Indeed, by increasing λ the left plate is cooled better and more heat is evacuated transversely in the channel resulting in increasingly higher temperatures near the cooled plate, and conversely for the nanoparticles volume fraction which migrate less towards this zone. Since the heat transfer takes place mainly in the transverse direction, improving the thermal conductivity in this direction by increasing λ has led to an enhancement of heat transfer rate on both channel walls. As for the previously considered parameters, the appearance of the reverse flow leads to a different thermal behavior in the vicinity of the heated wall where the increase of λ results in a reduction of Nu_{mh} . Indeed, for $\lambda \leq 0.75$ it is the flow acceleration near the heated wall, becoming more important by reducing λ , which controls the heat transfer. Whereas, for $\lambda > 0.75$ it is the increase of the transverse thermal conductivity which contributes more in convective transfer.

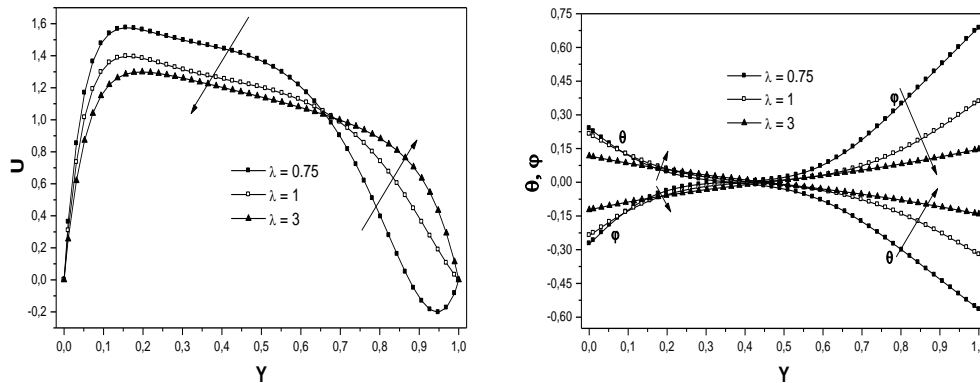


Figure 10: Profiles of U , θ and ϕ at channel exit for different values of λ , $Da=10^{-2}$, $Ri = 10$ and $R_q=1$

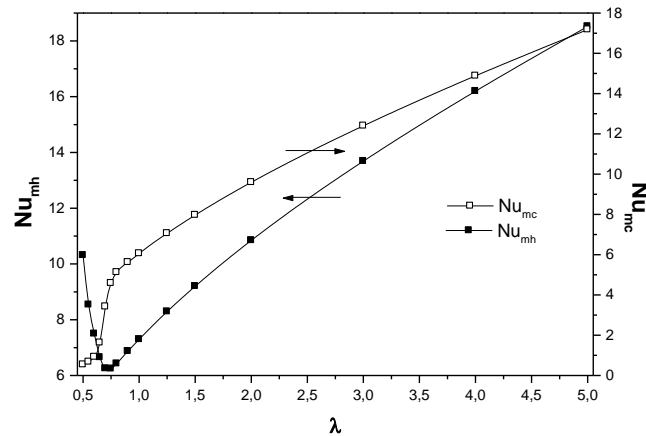


Figure 11: Variation of Nu_m with λ for $Da=10^{-2}$, $Ri=10$ and $R_q=1$

Fig. 12 gives the maps of reverse flow appearance as function of R_q , Ri , Da and λ . Knowing the conditions of occurrence of this flow is important to have either an improvement

(heated wall) or avoid a reduction (cooled wall) of heat transfer rates. The limit of appearance is far from being constant and varies with the parameters considered in this study. Thus at large heat flux ratio, the reverse flow occurs at low intensities of the buoyancy force, small porous medium permeabilities, and high values of the anisotropic thermal conductivity ratio.

An interesting result appears from the curve of Richardson number versus heat flux ratio. Comparing Fig. 3 and Fig. 6, Ri and R_q have the same tendency with one critical value for the reverse flow near the cold wall. Indeed, these two parameters are linked by the heated wall heat flux q_h and evolve in opposite directions with it so that $Ri \cdot R_q = \text{constant}$ for given values of Da and λ . This means that this constant is held either by increasing Ri and decreasing λ or vice versa. For the case of Fig. 12 with $Da=10^{-2}$ and $\lambda=1$, the critical value for the reverse flow appearance is approximately equal to 12.

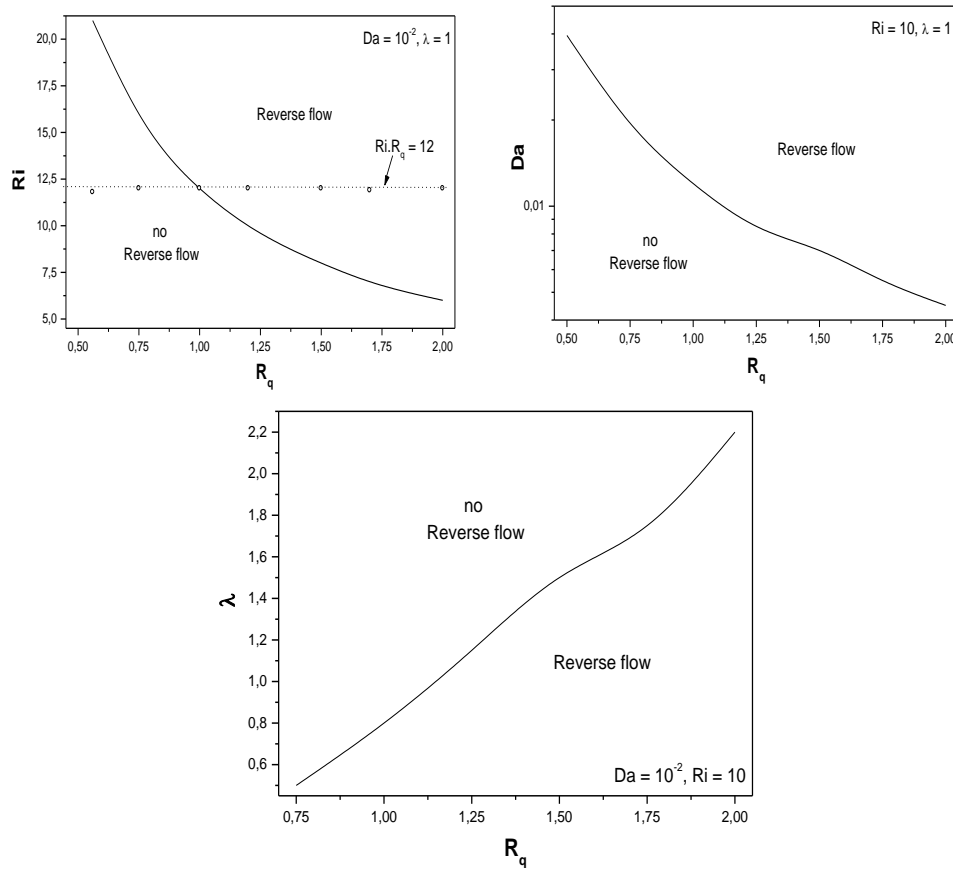


Figure 12: Maps of reverse flow appearance

5 Conclusion

The present study is a numerical investigation of mixed convection heat transfer of a nanofluid in a vertical channel filled by a thermally anisotropic porous medium with one wall heated and the other cooled.

-Axial velocity profiles and streamlines curves revealed that asymmetrical heating and buoyancy force are the most influential factors for occurrence of reverse flow.

-Reverse flow becomes stronger by increasing the buoyancy force strength, the porous medium permeability, the heat flux ratio and by decreasing the anisotropic thermal conductivity ratio.

- R_i and R_q have the same tendency with one critical value for the reverse flow near the cold wall characterized by R_i . $R_q=12$ for $Da=10^{-2}$ and $\lambda=1$.

-The non-uniform distribution of ϕ , resulting from migration of nanoparticles from the heated region to the cooled region, becomes more pronounced with the augmentation of R_i , Da , R_q and reduction of λ .

-Darcy number and thermal conductivity ratio have respectively decreasing and increasing effects on heat transfer rates for both channel walls. Nu_{mh} is enhanced with the augmentation of Richardson number and heat flux ratio, while Nu_{mc} evolves in opposite direction with these two control parameters. These behaviors become very noticeable with the appearance of reverse flow.

References

- Ameziani, D. E.; Bouhadeif, K.; Bennacer, R.; Rahli, O.** (2008): Analysis of the Chimney natural convection in a vertical porous cylinder. *Numbers Heat Transfer Part A*, vol. 54, pp. 47-66.
- Aung, W.; Worku, G.** (1986): Developing flow reversal in a vertical channel with asymmetric wall temperatures. *Journal of Heat Transfer-Transactions of the ASME*, vol. 108, pp. 299-304.
- Barletta, A.; Magyari, K.; Pop, I.; Storesletten, L.** (2008): Mixed convection with viscous dissipation in an inclined porous channel with isoflux impermeable walls. *Heat Mass Transfer*, vol. 44, pp. 979-988.
- Bera, P.; Khalili, A.** (2007): Stability of buoyancy opposed mixed convection in a vertical channel and its dependence on permeability. *Advances in Water Resources*, vol. 30, pp. 2296-2308.
- Buongiorno, J.** (2006): Convective transports in nanofluids. *Journal of heat transfer- transactions of the asme*, vol. 128, pp. 240-250.
- Chen, Y. C.; Chung, J. N.; Wu, C. S.; Lue, Y. F.** (2000): Non-Darcy mixed convection in a vertical channel filled with a porous medium. *International Journal of Heat and Mass Transfer*, vol. 43, pp. 2421-2429.
- Cheng, C. H.; Kou, H. S.; Huang, W. H.** (1990): Flow reversal and heat transfer of fully developed mixed convection in vertical channels. *Journal of Heat Transfer-Transactions of the ASME*, vol. 4, pp. 375-383.

- Choi, S. U. S.** (1995): Enhancing thermal conductivity of fluids with nano-particles. *Journal of Heat Transfer-Transactions of the ASME*, vol. 66, pp. 99-105.
- Cimpean, D.; Pop, I.; Ingham, D. B. Merkin, J. H.** (2009): Fully developed mixed convection flow between inclined parallel plates filled with a porous medium. *Transport in Porous Media*, vol. 77, pp. 87-102.
- Degan, G.; Vasseur, P.** (2002): Aiding mixed convection through a vertical anisotropic porous channel with oblique principal axes. *International Journal Engineering Science*, vol. 40, pp. 19-209.
- Desrayaud, G.; Lauriat, G.** (2009): Flow reversal of laminar mixed convection in the entry region of symmetrically heated, vertical plate channels. *International Journal of Thermal Sciences*, vol. 48, pp. 2036-2045.
- Fu, W. S.; Chao, W. S.; Wu, P. J.; Lin, Y. M.** (2016): A new method of adjustment of inlet boundary for improving heat transfer of mixed convection in a vertical channel. *International Communications in Heat and Mass Transfer*, vol. 77, pp. 165-173.
- Habib, M. A.; Said, S. A. M.; Ahmed, S. A.; Asghar, A.** (2002): Velocity characteristics of turbulent natural convection in symmetrically and asymmetrically heated vertical channels. *Experimental Thermal and Fluid Science*, vol. 26, pp. 77-87.
- Hadim, A.; Chen, G.** (1994): Non-Darcy mixed convection in a vertical porous channel with discrete heat sources at the walls. *International Communications in Heat and Mass Transfer*, vol. 21, pp. 377-387.
- Hajipour, M.; Dehkordi, A. M.** (2012): Analysis of nanofluid heat transfer in parallel-plate vertical channels partially filled with porous medium. *International journal of thermal sciences*, vol. 55, pp. 303-313.
- Jha, B. K.; Daramola, D.; Ajibade, A. O.** (2015): Mixed convection in an inclined channel filled with porous material having time-periodic boundary conditions: steady-periodic regime. *Transport in Porous Media*, vol. 109, pp. 495-512.
- Jha, B. K.; Daramola, D.; Ajibade, A. O.** (2016): Role of heat generation/absorption on mixed convection flow in a vertical tube filled with porous material having time-periodic boundary condition: steady-periodic regime. *Transport in Porous Media*, vol. 111, pp. 681-699.
- Kuznetsov, A. V.; Nield, D. A.** (2010): Natural convective boundary-layer flow of a nanofluid past a vertical plate. *International journal of thermal sciences*, vol. 49, pp. 243-247.
- Kuznetsov, A. V.; Nield, D. A.** (2014): Natural convective boundary-layer flow of a nanofluid past a vertical plate: a revised model. *International journal of thermal sciences*, vol. 77, pp. 126-129.
- Li, R.; Boussetta, M.; Chénier, E.; Lauriat, G.** (2013): Effect of surface radiation on natural convection flows and onset of flow reversal in asymmetrically heated vertical channels. *International Journal of Heat and Mass Transfer*, vol. 65, pp. 9-27.
- Maghrebi, M. J.; Nazari, M.; Armaghani, T.** (2012): Forced convection heat transfer of nanofluids in a porous channel. *Transport in Porous Media*, vol. 93, pp. 401-413.
- Malvandi, A.; Ganji, D. D.** (2014): Effects of nanoparticle migration on force convection of alumina/water nanofluid in a cooled parallel-plate channel. *Advanced Powder Technology*, vol. 25, pp. 1369-1375.

- Malvandi, A.; Ganji, D. D.** (2015): Effects of nanoparticle migration on hydromagnetic mixed convection of alumina/water nanofluid in vertical channels with asymmetric heating. *Physica E: Low-dimensional Systems and Nanostructures*, vol. 66, pp. 181-196.
- Matin, M. H.; Ghanbari. B.** (2014): Effects of Brownian motion and thermophoresis on the mixed convection of nanofluid in a porous channel including flow reversal. *Transport in Porous Media*, vol. 101, pp. 115-136.
- Nield, D. A.; Bejan, A.** (2013): *Convection in porous media. 4th Ed.* Springer, New York.
- Nield, D. A.; Kuznetsov, A. V.** (2009a): The Cheng-Minkowycz problem for natural convective boundary-layer flow in a porous medium saturated by a nanofluid. *International Journal of Heat and Mass Transfer*, vol. 52, pp. 5792-5795.
- Nield, D. A.; Kuznetsov, A. V.** (2009b): Thermal instability in a porous medium layer saturated by a nanofluid. *International Journal of Heat and Mass Transfer*, vol. 52, pp. 5796-5801.
- Nield, D. A.; Kuznetsov, A. V.** (2011a): The effect of vertical throughflow on thermal instability in a porous medium layer saturated by a nanofluid. *Transport in Porous Media*, vol. 87, pp. 765-775.
- Nield, D. A.; Kuznetsov, A. V.** (2011b): The Cheng-Minkowycz problem for the double-diffusive natural convective boundary layer flow in a porous medium saturated by a nanofluid. *International Journal of Heat and Mass Transfer*, vol. 54, pp. 374-378.
- Nield, D. A.; Kuznetsov, A. V.** (2011c): The onset of double-diffusive convection in a nanofluid layer. *International Journal of Heat and Mass Transfer*, vol. 32, pp. 771-776.
- Patankar, S. V.** (1980): *Numerical heat transfer and fluid flow.* McGraw-Hill, New York.
- Sheremet, M. A.; Pop, I.** (2014): Conjugate natural convection in a square porous cavity filled by a nanofluid using Buongiorno's mathematical model. *International Journal of Heat and Mass Transfer*, vol. 79, pp. 181-196.
- Shivakumara, I. S.; Dhananjaya, M.** (2015): Penetrative Brinkman convection in an anisotropic porous layer saturated by a nanofluid. *Ain Shams Engineering Journal*, vol. 6, pp. 703-713.
- Sparrow, E.; Chrysler, G.; Azevedo, L.** (1984): Observed flow reversals and measured-predicted Nusselt numbers for natural convection in a one-sided heated vertical channel. *Journal of Heat Transfer-Transactions of the ASME*, vol. 106, pp. 325-332.
- Umavathi, J. C.; Kumar, J. P.; Chamkha, A. J.; Pop, I.** (2005): Mixed convection in a vertical porous channel. *Transport in Porous Media*, vol. 61, pp. 315-335.
- Xu, H.; Fan, T.; Pop, I.** (2013): Analysis of mixed convection flow of a nanofluid in a vertical channel with the Buongiorno mathematical model. *International Communications in Heat and Mass Transfer*, vol. 44, pp. 15-22.
- Yang, C.; Li, W.; Nakayama, A.** (2013): Convective heat transfer of nanofluids in a concentric annulus. *International journal of thermal sciences*, vol. 71, pp. 249-257.